Am J Physiol Heart Circ Physiol 289: H270–H276, 2005.
First published February 18, 2005; doi:10.1152/ajpheart.00636.2003.

Wave-energy patterns in carotid, brachial, and radial arteries: a noninvasive approach using wave-intensity analysis

A. Zambanini,[1] S. L. Cunningham,[1] K. H. Parker,[2] A. W. Khir,[2] S. A. McG. Thom,[1] and A. D. Hughes[1]

[1] *Department of Clinical Pharmacology, Faculty of Medicine, St. Mary's Hospital; and* [2]*Physiological Flow Studies Group, Department of Bioengineering, Imperial College, London, United Kingdom*

Submitted 15 August 2003; accepted in final form 1 February 2005

Zambanini, A., S. L. Cunningham, K. H. Parker, A. W. Khir, S. A. McG. Thom, and A. D. Hughes. Wave-energy patterns in carotid, brachial, and radial arteries: a noninvasive approach using wave-intensity analysis. *Am J Physiol Heart Circ Physiol* 289: H270–H276, 2005. First published February 18, 2005; doi:10.1152/ajpheart.00636.2003.—The study of wave propagation at different points in the arterial circulation may provide useful information regarding ventriculoarterial interactions. We describe a number of hemodynamic parameters in the carotid, brachial, and radial arteries of normal subjects by using noninvasive techniques and wave-intensity analysis (WIA). Twenty-one normal adult subjects (14 men and 7 women, mean age 44 ± 6 yr) underwent applanation tonometry and pulsed-wave Doppler studies of the right common carotid, brachial, and radial arteries. After ensemble averaging of the pressure and flow-velocity data, local hydraulic work was determined and a pressure-flow velocity loop was used to determine local wave speed. WIA was then applied to determine the magnitude, timings, and energies of individual waves. At all sites, forward-traveling (S) and backward-traveling (R) compression waves were observed in early systole. In mid- and late systole, forward-traveling expansion waves (X and D) were also seen. Wave speed was significantly higher in the brachial (6.97 ± 0.58 m/s) and radial (6.78 ± 0.62 m/s) arteries compared with the carotid artery (5.40 ± 0.34 m/s; $P < 0.05$). S-wave energy was greatest in the brachial artery (993.5 ± 87.8 mJ/m^2), but R-wave energy was greatest in the radial artery (176.9 ± 19.9 mJ/m^2). X-wave energy was significantly higher in the brachial and radial arteries (176.4 ± 32.7 and 163.2 ± 30.5 mJ/m^2, respectively) compared with the carotid artery (41.0 ± 9.4 mJ/m^2; $P < 0.001$). WIA illustrates important differences in wave patterns between peripheral arteries and may provide a method for understanding ventriculoarterial interactions in the time domain.

hemodynamics; wave transmission; ultrasound; tonometry

THE MAINTENANCE OF PRESSURE GRADIENTS and blood flow in the arterial circulation is mediated through complex hemodynamic interactions resulting from energy transfer between the heart and arteries (23). The heart generates forward-traveling wave energy that propagates through the arteries to maintain tissue and organ perfusion for metabolic homeostasis.

An individual forward-traveling wavefront, generated by the heart at the beginning of cardiac systole, initiates flow and increases pressure in the arteries (25). Although most of the wave energy in this initial compression wave travels distally into smaller arteries, some is reflected back toward the heart at sites of impedance mismatch. These include focal sites such as bifurcations, but nonfocal arterial taper may also contribute to reflection phenomena (39). These reflected waves can be rereflected as has been demonstrated in vitro (19). At the end of systole, deceleration of left ventricular contraction results in reductions in both pressure and flow in the ascending aorta mediated by a forward-traveling expansion wave (34).

Interactions between forward- and backward-traveling waves result in complex patterns of blood flow and pressure change at different points in the arterial circulation. Analysis of forward- and backward-traveling wave energy therefore provides information regarding ventriculoarterial interaction (8, 10, 35).

The study of arterial waves has classically used vascular impedance theory that considers the observed pressure and flow waveforms to be the superposition of sinusoidal wave trains at the fundamental and harmonic frequencies (26). This method, based on Fourier theory, assumes a linear relationship between pressure and flow in a one-dimensional system at steady state (32). An alternative approach uses the method of characteristics, which considers the measured waveforms as the summation of successive incremental wave fronts. The method assumes neither periodicity nor linearity but does assume waves to be one dimensional in character (33). This has resulted in the development of wave-intensity analysis (WIA) as a novel mathematical tool to describe arterial wave power and energy.

Wave intensity is a term analogous to acoustic intensity and is defined as power transported by the wave fronts per unit area. Changes in pressure and flow velocity are used to determine wave intensity, and the method also allows local wave speed to be determined. Furthermore, with the use of the local wave speed determined from a pressure-flow velocity loop (18), WIA allows the separation of forward- and backward-traveling waves. By referring to the concomitant changes in pressure, compression and expansion can be described (9). Compression and expansion waves have opposite effects on pressure and flow velocity (Table 1).

To date, most of the published studies using WIA to study arterial waves have acquired simultaneous pressure and flow data using invasive methods (9, 11, 20, 22, 33, 35). Most studies have focused on cardiac or aortic hemodynamics rather than studying waves in more peripheral arteries. Three studies performed at the carotid artery, using noninvasive techniques, have used the arterial diameter change waveform over time rather than a directly measured arterial pressure waveform for the analysis (28–30). None of the noninvasive studies separated the arterial waves into their forward- and backward-traveling components.

With the advent of applanation tonometry and pulsed-wave Doppler, it is now possible to measure both arterial pressure

Address for reprint requests and other correspondence: A. Hughes, Dept. of Clinical Pharmacology, 10th Floor QEQM, St. Mary's Hospital, London W2 1NY, UK (E-mail: a.hughes@imperial.ac.uk).

The costs of publication of this article were defrayed in part by the payment of page charges. The article must therefore be hereby marked "*advertisement*" in accordance with 18 U.S.C. Section 1734 solely to indicate this fact.

Table 1. *Effects of forward- and backward-traveling compression and expansion waves on local pressure and flow velocity*

	Compression	Expansion
Forward	Flow velocity ↑ Pressure ↑	Flow velocity ↓ Pressure ↓
Backward	Flow velocity ↓ Pressure ↑	Flow velocity ↑ Pressure ↓

(13, 15, 16, 21, 25) and flow velocity (4, 37) noninvasively and reproducibly in superficial peripheral arteries. The aim of this study is to describe wave intensity and energy patterns in the carotid, brachial and radial arteries of normal human subjects by using noninvasive methods.

MATERIALS AND METHODS

Subjects. The study was approved by the St. Mary's Hospital Research Ethics Committee. All subjects were healthy nonsmokers, and excluded were volunteers with a previous history of cardiovascular, cerebrovascular or peripheral vascular disease, hypertension, diabetes, or dyslipidaemia. Subjects currently taking vasoactive medication were also ineligible for the study.

Data acquisition. All the methods used for this study have been described fully in a previous work (43). In brief, subjects were examined while lying supine on a couch in a quiet, temperature-controlled room after a ~10-min rest period. At least three measures of left arm brachial artery systolic (SBP) and diastolic blood pressure (DBP) were then acquired during the study by using a validated, semiautomated blood pressure monitor (Omron HEM-705CP, Hoofddorp, The Netherlands) (31). Mean arterial blood pressure (MAP) was calculated from the standard formula MAP = DBP + (SBP − DBP)/3 (41).

To standardize the protocol, data from the common carotid, brachial, and radial arteries on the right side were collected in the same sequence in all patients. At each site the pressure data were collected first, followed by the velocity data before progressing to the next artery. For each artery, the time taken to acquire both pressure and velocity data was ~5 min.

Applanation tonometry was used to record arterial pressure waveforms from the three arteries by using a high-fidelity strain gauge-tipped pencil probe (2). The areas of maximum pulsation were identified by palpation for each of the three arteries, and the tonometer (SPT 301, Millar Instruments, Houston, TX) was then applied to these sites. Over a period of at least 20 cardiac cycles, the signal was amplified (TCB-500 preamplifier, Millar Instruments), digitized at 200 Hz, and transferred to the hard drive of a personal computer (PC) for further analysis. A simultaneous single-lead ECG was also recorded.

To acquire flow-velocity data from the three arteries, the common carotid, brachial, and radial arteries on the right side were imaged using a 7.5- to 10-MHz linear-array transducer and HDI5000 ultrasound machine (ATL-Philips, Bothell, WA). At all sites, B-mode ultrasound was used to ensure correct positioning of the transducer, and pulsed-wave Doppler ultrasound, with a fundamental frequency of 6 MHz, was used to insonate the arterial lumen while ensuring that the ultrasound beam was positioned at 60° incident to the direction of the central luminal blood flow (45). The pulsed Doppler velocity waveform and a simultaneous single-lead ECG trace were acquired continuously for 20 cardiac cycles. A peak velocity waveform was generated using a well-described, online tracing algorithm (36, 38), digitized at a frequency of 200 Hz, and then transferred to a PC hard drive. At each site, the flow-velocity data were acquired within 5 min of the corresponding pressure data.

Ensemble averaging of the pressure and flow-velocity data. To provide simultaneous representative pressure and flow-velocity waveforms, ensemble averaging of the acquired pressure and flow-velocity data was performed within the Matlab programming environment (Matlab 6.0.0.88 Release 12, MathWorks, Natick, MA). Six contiguous pressure and flow-velocity waveforms were separated using the fiducial ECG R wave and then ensemble averaged. Ensemble averaging was performed by maximizing the cross-correlation coefficient between each waveform using the first 100 ms of the rapid rise in pressure and flow velocity with a facility for subsequent manual adjustment if necessary.

Calibration of the ensemble-averaged carotid pressure waveform was performed indirectly (43, 44). Previous work (43, 44) has shown that the applanation tonometer may either under or overestimate intra-arterial pressure depending on the force used for applanation. In addition, when MAP alone was used to calibrate the pressure waveforms obtained from our tonometer in vivo, then the waveform pulse pressure differed 13–41% from sphgmomanometry, depending on the patient group studied. We therefore calibrated our tonometer using a pressure phantom.

A pressure phantom was constructed using 1-cm-diameter latex tube placed within a similarly sized Dacron graft. An intravascular pressure catheter (8F SVPC-684A, Millar Instruments) was introduced into the phantom, and the system was filled with saline to achieve a static pressure of 50 mmHg. The high-fidelity strain-gauge tonometer was externally placed 1 cm distal to the catheter and attached to a stand for hands-free measurements. Rapid active filling and passive drainage of the phantom using saline and a syringe achieved variations in pressure. The pressure data from tonometry and invasive catheter measurements were sampled simultaneously at 250 Hz. A series of pressure waveforms was generated over a range of applied applanation pressures. These data confirmed that there was a linear relationship between the intraluminal catheter and tonometry pressures but that the slope of linear regression line increased linearly with an increase in applanation pressure. From these data, appropriate calibration of the tonometer was feasible, thus taking into account the applied force required for applanation.

In vivo, the average applanation force was determined from the six pressure waveform data before ensemble averaging, using the average difference in the measured carotid diastolic pressures (determined by the tonometer) and the brachial DBP (determined by sphygmomanometry). These data were then applied to the pressure data to correct for the applanation force-dependent error (43, 44). A final step matched the ensemble-averaged carotid mean arterial pressure to MAP. Brachial and radial pressure waveforms were ensemble averaged and calibrated directly to the measured brachial SBP and DBP. Whereas the magnitude and morphology of the brachial and radial pressure waveforms are not identical, calibration of the radial pressure waveform using syphgmomanometry-determined brachial SBP and DBP is well established in the literature (12, 14), and the neglect of amplification of the pressure wave between the brachial and radial arteries introduces only a very minor error (24).

Doppler may overestimate peak flow velocities, and errors, particularly at low forward and backward velocities, vary in a nonlinear manner, resulting in distortion of the temporal characteristics of the flow-velocity waveform (34). This may be of particular importance in the brachial, radial, and femoral arteries where flow reversal might typically occur during the cardiac cycle. The nonlinear errors were attributed to the statistical properties of the online velocity waveform-tracing algorithm, and a formula for correction was therefore developed in vitro using a string phantom and shaft encoder. Nonlinear regression analysis, based on a cumulative standard normal probability distribution, was used to determine an appropriate correction. When applied to data in the string phantom that mimicked physiological flow-velocity waveforms, there was a close correlation between the corrected velocities and those determined independently by

the shaft encoder ($r^2 = 0.99$, $P < 0.0001$), and the nonlinear errors were no longer evident.

In vivo, following application of the correction formula determined in the string phantom experiments, six contiguous flow-velocity waveforms were separated in the same manner as the pressure data. Similarly, these data were ensemble averaged after each waveform was aligned using the first 100 ms of the rapid rise in flow velocity as described above to generate a single ensemble-averaged flow-velocity waveform (U).

Hemodynamic calculations. Hydraulic work per unit area was calculated as:

$$W = \int_0^T \mathrm{P}U\mathrm{d}t \qquad (1)$$

where T represents the average duration of the ensemble averaged cardiac cycle, P represents pressure, and dt is the sampling interval (5 ms).

Local wave speed was calculated using a pressure-flow velocity loop (18). From the conservation of mass and momentum, there is a simple relationship between the changes in pressure and flow velocity that is valid only when a forward-traveling wave is present, and this is summarized in the "waterhammer" equation:

$$\mathrm{dP}_{\pm} = \rho c \mathrm{d}U_{\pm} \qquad (2)$$

where dP is the measured change in pressure over one sampling period, $\pm$ is forward and backward, dU is the measured change in flow velocity over one sampling period, + is forward and − is backward, ρ is the density of blood (1.06 g/cm^3), and c is the local wave speed. If the ensemble-averaged pressure and velocity data are plotted as shown in Fig. 1, a pressure-flow velocity loop can be constructed. In the carotid artery there is a linear portion of the loop corresponding to the earliest part (~50 ms) of arterial systole. This suggests that during this time there are no reflected waves present at the site of measurement. During this early period of arterial systole, ρc is equal to the gradient of the line describing the relationship between pressure and flow velocity, and, using *Eq. 2*, local wave speed can be calculated. At the brachial and radial arteries where earlier reflections may occur, the gradient of the early linear portion of the loop was determined over the first 15 ms of arterial systole.

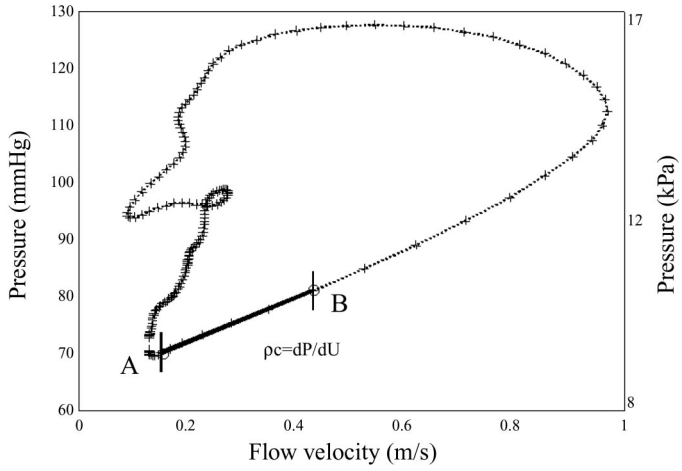

Fig. 1. Pressure-flow velocity loop constructed from data acquired from the common carotid artery in a single individual, where ρ is blood density; c is local wave speed; dP is measured change of pressure over one sampling period; and dU is measured change in flow velocity over one sampling period. The part of the curve marked in bold (A and B) is the area from which the gradient is calculated to determine wave speed (once pressure is converted to N/m^2). Each data point is acquired by using a sampling interval of 5 ms. The start and end of the cardiac cycle (A) represents the lower lefthand corner of the loop as marked and time progresses in an counterclockwise fashion.

Table 2. *Clinical characteristics of normal subjects participating in the study*

Gender	14 Men, 7 Women
Age, yr	44 (SD 6)
Brachial SBP, mmHg	115 (SD 10)
Brachial DBP, mmHg	73 (SD 6)
Heart rate, beats/min	65 (SD 9)
Height, m	1.71 (SD 0.10)
Weight, kg	74.2 (SD 12.7)
Body mass index, kg/m^2	25.2 (SD 2.9)

Data are means ± SD. SBP, systolic blood pressure; DBP, diastolic blood pressure.

The pressure-flow velocity loop was also used to ensure that the pressure and flow-velocity data were appropriately aligned as these data had been acquired sequentially. Although the fiducial ECG R wave had been used to separate individual pressure and flow-velocity waveforms before ensemble averaging, small differences (±5 ms) in the alignment of P and U were sometimes evident. In such cases, alignment was corrected by shifting the flow-velocity data forward or backward by 5 ms with reference to the pressure data to ensure a linear relationship between pressure and flow velocity during their initial increase (Fig. 1).

The mathematical methods of WIA are described in more detail in previous work (11, 33). The forward and backward components of the measured change in pressure and flow velocity were determined from the following equations derived from the method of characteristics theory:

$$\text{Change in pressure: } \mathrm{dP}_{\pm} = 1/2(\mathrm{dP} \pm \rho c \mathrm{d}U) \qquad (3)$$

$$\text{Change in flow velocity: } \mathrm{d}U_{\pm} = 1/2(\mathrm{d}U \pm \mathrm{dP}/\rho c) \qquad (4)$$

With the integration of the forward- and backward-traveling changes in pressure, the forward- and backward-pressure waveforms were determined, and, from these, maximum forward and backward pressure could be calculated. An integration constant was included arbitrarily in the forward pressure and was taken to be the minimum value of P. The integration constant for U was zero.

Forward and backward wave intensities (I) were calculated as follows:

$$\mathrm{d}I_{\pm} = \mathrm{dP}_{\pm}\mathrm{d}U_{\pm} \qquad (5)$$

Forward wave intensities had a magnitude greater than zero, whereas backward wave intensities had a magnitude less than zero.

Compression waves were defined as occurring during positive changes in pressure and expansion waves during negative changes. The time of onset and offset of each wave was determined manually using electronic crosshairs, and the error in timings was <5 ms. Wave energy was determined by integrating the area under the wave-intensity curve between these two time points. The time of onset of each wave was determined relative to the onset of the first forward compression wave (S). The time of onset of the S wave relative to the fiducial ECG R wave was also determined.

Other groups have normalized wave intensity as the product of the derivatives of P and U with respect to time (dP/dt and dU/dt, respectively) (11, 35). Such an approach allows data acquired at different sampling rates to be compared directly but results in complex units (mmHg·m·s^{-3}), which do not represent wave power per unit area and do not allow wave energy to be easily determined. To compare the results from this study with those from other groups, one should convert watts per squared meter into millimeters of Hg times meter per cubed seconds by multiplying wave intensity values by 300. Previous studies have not separated the waves into their forward- and

Table 3. *Maximum forward and backward components of pressure and pulse pressure in the carotid, brachial, and radial arteries*

	Carotid	Brachial	Radial
Maximum forward pressure	98±2	106±2‡	101±2
Forward pulse pressure	23±1	33±2‡	28±2*
Maximum backward pressure and pulse pressure	11±1	14±1†	15±1*

Data are means ± SE in mmHg. The maximum forward pressure includes the integration constant (minimum arterial pressure). *$P < 0.05$, †$P < 0.01$, ‡$P < 0.001$.

backward-traveling components and have therefore only reported net wave intensity.

Statistics. The clinical characteristics of the subjects are expressed as means ± SD, whereas all other data, which are derived from ensemble-averaged pressure and flow velocity, are expressed as means ± SE. To assess the significance of differences between arterial sites, two-way ANOVA was used (Excel, Microsoft Office 2000, Microsoft, Redmond, WA). The *F*-statistic and *P* values are presented, and *P* values were considered significant at values <0.05.

RESULTS

The baseline characteristics of the 21 normal subjects that participated in the study are shown in Table 2. Systolic pressures in the brachial and radial arteries were significantly higher than that in the carotid artery (115 ± 2 mmHg, brachial and radial; 106 ± 2 mmHg, carotid; $F = 161.8$, $P < 0.001$). However, diastolic pressure was significantly higher in the carotid artery compared with the other two sites (75 ± 1 mmHg, carotid; 73 ± 1 mmHg, brachial and radial; $F = 11.4$, $P < 0.005$). Heart rate was similar during the studies at all three sites (carotid, 61 ± 2 beats/min; brachial, 64 ± 2 beats/min; and radial, 64 ± 2 beats/min).

Wave speed was significantly higher in the brachial (6.97 ± 0.58 m/s) and radial (6.78 ± 0.62 m/s) arteries compared with the carotid artery (5.40 ± 0.34 m/s) (brachial vs. carotid, $F = 7.5$, $P = 0.01$, and radial vs. carotid, $F = 4.1$, $P < 0.05$), but the difference in wave speed between the brachial and radial arteries was not significant ($F = 0.0$, $P = 0.9$).

Hydraulic work was significantly higher in the carotid artery (539 ± 27 J/m^2) compared with the brachial (315 ± 45 J/m^2) and radial (251 ± 46 J/m^2) arteries (carotid vs. brachial, $F = 24.3$, $P < 0.001$, and carotid vs. radial, $F = 38.6$, $P < 0.001$). There was no significant difference in hydraulic work between the brachial and radial arteries ($F = 3.5$, $P = 0.09$).

The maximum forward and backward components of pressure and pulse pressure are shown in Table 3. Forward pressure was significantly higher in the brachial artery compared with the carotid artery ($F = 163.4$, $P < 0.001$). Taking into account the integration constant in the forward pressure, the forward pulse pressures were significantly higher in both the brachial ($F = 253.2$, $P < 0.001$) and radial arteries ($F = 6.4$, $P < 0.05$) compared with the carotid artery. Additionally, maximum reflected backward pressures and backward pulse pressures were significantly higher in the brachial ($F = 14.7$, $P < 0.005$) and radial arteries ($F = 6.9$, $P < 0.05$) compared with the carotid artery.

Figure 2 illustrates the relationships among pressure, flow velocity, and wave intensities in the carotid, brachial, and radial arteries of a typical normal subject. In the carotid artery, an early systolic S wave was associated with a rapid rise in pressure and flow velocity at the beginning of systole. A small, reflected compression R wave (R) from the head resulted in

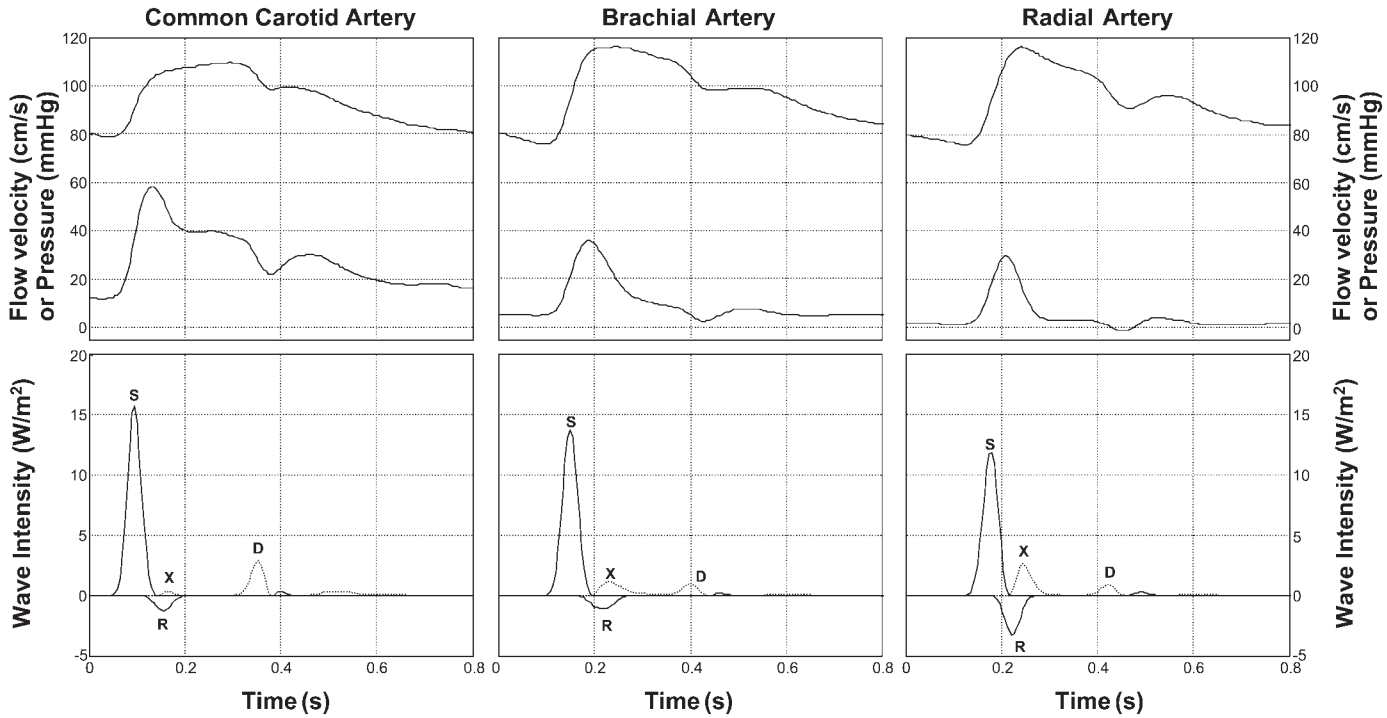

Fig. 2. Pressure, flow velocity, and wave intensities in the carotid, brachial,and radial arteries from a single volunteer. *Top*: pressure is *top* waveform and flow velocity is *bottom* waveform. *Bottom*: forward-traveling compression wave (S), backward-traveling compression wave (R), and two forward traveling expansion waves (X, D).

Table 4. *Individual peak wave intensities and wave energies at the carotid, brachial, and radial arteries*

	Carotid		Brachial		Radial	
Wave	d*I*, W/m^2	Energy, mJ/m^2	d*I*, W/m^2	Energy, mJ/m^2	d*I*, W/m^2	Energy, mJ/m^2
S	16.76±1.53	616.9±55.0	22.34±2.01†	993.5±87.8†	16.30±1.70‡	747.8±77.5
R	2.18±0.39	108.9±15.9	2.16±0.40	141.1±22.8	3.21±0.38‡	176.9±19.9*
X	1.04±0.23	41.0±9.4	3.22±0.65†	176.4±32.7†	3.09±0.56†	163.2±30.5†
D	2.12±0.17	75.7±5.0	1.59±0.23*	74.4±12.8	1.09±0.13†	53.4±7.0†

Data for individual peak wave intensities (d*I*) and wave energies are means ± SE. *$P < 0.05$; †$P < 0.01$ compared with the carotid artery; ‡$P < 0.05$ compared with the brachial artery.

pressure augmentation and a reduction in flow velocity. Further deceleration of flow and a reduction in local pressure was associated with the presence of a forward-traveling expansion wave (X), and further reduction in pressure and flow velocity at the end of systole occurred in association with another forward-traveling expansion wave (D). There was a similar pattern of forward and backward waves in both the brachial and radial arteries, although R waves at these sites were reflected waves from the lower arm and hand, respectively.

Table 4 shows the mean wave intensities and energies for waves S, R, X, and D in each of the three arteries. The S-wave intensity was significantly higher at the brachial artery compared with the carotid and radial arteries. Additionally, S-wave energy was significantly higher in the brachial artery compared with the carotid artery. However, R-wave energy was significantly higher in the radial artery compared with the carotid artery. The X-wave intensity and energy were significantly lower in the carotid artery compared with both the brachial and radial arteries. The D-wave intensity was significantly higher in the carotid and brachial arteries compared with the radial artery. D-wave energy was significantly higher in the carotid artery compared with the radial artery.

The S wave occurred earlier in the carotid artery (77 ± 3 ms relative to the ECG R wave) compared with the brachial (122 ± 3 ms) and radial (143 ± 3 ms) arteries. Table 5 shows the differences in the timing of onset of the R, X, and D waves relative to the S wave at each of the three arteries. The onset of the R wave occurred significantly later in the carotid artery compared with the brachial ($F = 6.6$, $P < 0.05$) and radial arteries ($F = 17.3$, $P < 0.001$). The X wave occurred earlier in the carotid artery compared with the brachial artery ($F = 13.5$, $P < 0.01$), although there were no significant differences between the brachial and the radial arteries. There were no significant differences between the sites in the timing of onset of the D wave.

DISCUSSION

This study has shown that wave patterns, as determined using WIA, differ between peripheral arteries. The broad pattern of forward- and backward-transmitted waves was relatively similar in the carotid, brachial, and radial arteries, and four distinct waves (S, R, X, and D) were identifiable at each site in every individual. Previous work (20) acquiring invasive data from the ascending aorta in humans showed some similarities in the pattern of wave transmission to that seen in the carotid artery, although a midsystolic X wave was not reported, suggesting this seldom or never occurs in the ascending aorta.

Table 5. *Delay of the onset of the R, X, and D waves relative to the time of onset of the S wave in the carotid, brachial, and radial arteries*

	Carotid	Brachial	Radial
R	56±3	43±6	32±4
X	106±2	116±3	116±2
D	248±5	247±6	251±6

Data are means ± SE, in ms.

Both the S and D waves are generated by the left ventricle of the heart (10, 34). The S wave is generated by myocardial contraction, resulting in the opening of the aortic valve, increased arterial pressure, and acceleration of arterial flow. In this study, we showed that both the S-wave intensity and the forward component of pressure were significantly higher in the brachial artery compared with the carotid artery. A reasonable assumption, bearing in mind the similarity in heart rates during the brachial and carotid studies, is that cardiac contractility remained unchanged during these studies. The differences in wave power between the two sites may therefore have been mediated through differences in arterial wall structure, geometry, and branching. For example, from *Eq. 2* it can be seen that as local wave speed increases, the forward component of pressure can be predicted to increase.

The D wave is an expansion wave generated at the end of systole by a decrease in myocardial shortening rate that results in a reduction in both arterial pressure and flow and contributes to the closure of the aortic valve. We have shown that D-wave intensity differs between the carotid and more peripheral arteries, being highest in the carotid artery and lowest in the radial artery. Importantly, we note that the timing of the wave is the same in all three arteries relative to the S wave, confirming previous work suggesting that the wave is of cardiac origin. The D wave may become smaller in magnitude as it travels distally from the heart due to damping by the arterial wall and therefore contributes less to pressure and flow reduction at the end of systole in the smaller muscular arteries compared with the central elastic arteries, such as the carotid and aorta arteries.

The R wave is a backward-traveling reflection of the S wave. Previous in vivo work using aortic clamping or aortic balloon inflation to increase the local reflections has resulted either in an increase in the R-wave intensity (35) or earlier onset and longer duration of the R wave (17) in the ascending aorta. These changes have been associated with augmentation of pressure or an increase in hydraulic work in the ascending aorta.

We showed that R-wave energy was significantly higher in the radial artery compared with that in the carotid artery and that the peak-reflected backward pressure was significantly

higher from the hand and forearm than from the head. By normalizing for the S-wave energy in each artery, it is apparent that there are differences in the amount of reflection at each site. For example ~17% of the S-wave energy was reflected as the R wave in the carotid artery compared with 27% in the radial artery. This indicates that there are differences in impedance mismatching between different beds, and the increased reflection from the hand may be related either to the anatomy of the hand circulation or the level of resting vasoconstrictor tone in the hand where circulation largely occurs through the skin.

Our study is the first to describe the presence of midsystolic X waves in peripheral arteries. Previous studies have shown the presence of reflected, backward-traveling expansion waves in the pulmonary arteries during early systole (7) and in the coronary arteries during early diastole (42), and these resulted in a reduction in pressure and an increase in flow velocity. However, the X wave is a forward-traveling expansion wave that contributes to a reduction in both pressure and flow velocity during midsystole. The heart is unlikely to be the source of the X wave. Previous invasive work has not observed X waves in the ascending aorta. Additionally, our data show that the X-wave energy is higher at a more peripheral site (the radial artery) compared with a more central artery (the carotid artery). The X wave may therefore occur after reflection of the R wave from a proximal open-end type reflection site, such as when it travels back toward the heart and meets a bifurcation (7, 27).

The differences in hydraulic work and wave speed between elastic and muscular arteries are representative of differences in their structure and function. Typically, the brain receives ~15% of cardiac output (5), and, assuming that the majority of cerebral blood flow travels via the carotid arteries, each carotid artery carries ~7% of cardiac output. The brachial artery, however, receives a much smaller proportion of the cardiac output at rest. Estimates from our data suggest that the forearm receives ~2% of the cardiac output at rest. Thus one might expect hydraulic work in the carotid artery to be greater than that in the brachial and radial arteries in the resting state.

Wave speed is dependent on the elastic properties of the wall, wall thickness, the luminal radius, the Poisson ratio (the ratio of transverse to longitudinal strain), and the density of blood (1). The distensibility of an artery (Δ) (defined as $1/A \cdot dA/dP$, where A is the cross-sectional area in arterial diastole and dA is the change in cross-sectional area), has a simple relationship to the wave speed ($c = 1/\sqrt{\rho\Delta}$). Structural factors that influence arterial distensibility clearly influence the local wave speed. Histological work has described the structural differences between elastic and muscular arteries (3, 6) and recent noninvasive work (40) confirms that the elastic moduli of the brachial and radial arteries are different to that of the common carotid artery.

Potential limitations. The use of noninvasive methods is important to assess arterial hemodynamics in both healthy volunteers and in patient groups, because invasive monitoring is increasingly becoming ethically unacceptable, particularly in our institution. This inevitably introduces potential sources of error. For example, in our study we acquired pressure and flow-velocity data sequentially, whereas in previous invasive studies these data were acquired simultaneously using appropriate catheters. Furthermore, the calibration of the pressure waveform required the use of noninvasively acquired data. However, brachial sphygmomanometry, a tool widely used and accepted in routine clinical practice, provides accurate estimates of brachial blood pressure, provided there is no evidence of calcification of the media of the artery. In this study, direct imaging of the arterial wall was performed in every subject.

A potential source of error was the calibration of the radial pressure directly to the brachial sphygmomanometry pressure. Although this may introduce a small error, this strategy has been applied in a number of previous studies (12, 14).

In conclusion, we have described important differences in wave speed, hydraulic work, and wave patterns among the carotid, brachial, and radial arteries of normal volunteers using noninvasive techniques. Wave transmission in peripheral arteries is a complex interaction of forward- and backward-traveling compression and expansion waves produced by the heart or generated by reflections.

REFERENCES

1. **Bergel DH.** The dynamic elastic properties of the arterial wall. *J Physiol (Lond)* 156: 458–469, 1961.
2. **Drzewiecki GM, Melbin J, and Noordergraaf A.** Arterial tonometry: review and analysis. *J Biomech* 16: 141–152, 1983.
3. **Fischer GM and Llaurado JG.** Collagen and elastin content in canine arteries selected from functionally different vascular beds. *Circ Res* 19: 394–399, 1966.
4. **Fischer M and Alexander K.** Reproducibility of carotid artery Doppler frequency measurements. *Stroke* 16: 973–976, 1985.
5. **Guyton AC.** The autonomic nervous system: cerebral blood flow and cerebrospinal fluid. In: *Human Physiology and Mechanisms of Disease*. Philadelphia, PA: Saunders, 1992, p. 459–471.
6. **Harkness MLR, Harkness RD, and McDonald DA.** The collagen and elastin content of the arterial wall in the dog. *Proc Roy Soc Lond* 146B: 541–551, 1957.
7. **Hollander EH, Wang JJ, Dobson GM, Parker KH, and Tyberg JV.** Negative wave reflections in pulmonary arteries. *Am J Physiol Heart Circ Physiol* 281: H895–H902, 2001.
8. **Jones CJ, Goodfellow J, Bleasdale RA, and Frenneaux MP.** Modulation of interaction between left ventricular ejection and the arterial compartment: assessment of aortic wave travel. *Heart Vessels* 15: 247–255, 2000.
9. **Jones CJ, Parker KH, Hughes R, and Sheridan DJ.** Nonlinearity of human arterial pulse wave transmission. *J Biomech Eng* 114: 10–14, 1992.
10. **Jones CJ and Sugawara M.** "Wavefronts" in the aorta—implications for the mechanisms of left ventricular ejection and aortic valve closure. *Cardiovasc Res* 27: 1902–1905, 1993.
11. **Jones CJ, Sugawara M, Davies RH, Kondoh Y, Uchida K, and Parker KH.** Arterial wave intensity: physical meaning and physiological significance. In: *Recent Progress in Cardiovascular Mechanics*. London: Harwood Academic, 1994, p. 129–148.
12. **Kelly R, Daley J, Avolio A, and O'Rourke M.** Arterial dilation and reduced wave reflection. Benefit of dilevalol in hypertension *Hypertension* 14: 14–21, 1989.
13. **Kelly R and Fitchett D.** Noninvasive determination of aortic input impedance and external left ventricular power output: a validation and repeatability study of a new technique. *J Am Coll Cardiol* 20: 952–963, 1992.
14. **Kelly R, Hayward C, Avolio A, and O'Rourke M.** Noninvasive determination of age-related changes in the human arterial pulse. *Circulation* 80: 1652–1659, 1989.
15. **Kelly R, Hayward C, Gains J, Daley J, Avolio A, and O'Rourke M.** Noninvasive registration of the arterial pressure waveform using high-fidelity applanation tonometry. *J Vasc Med Biol* 1: 142–149, 1989.
16. **Kelly R, Karamanoglu M, Gibbs H, and O'Rourke M.** Noninvasive carotid pressure wave registration as an indicator of ascending aortic pressure. *J Vasc Med Biol* 1: 241–247, 1989.
17. **Khir AW, Henein MY, Koh T, Das SK, Parker KH, and Gibson DG.** Arterial waves in humans during peripheral vascular surgery. *Clin Sci (Lond)* 101: 749–757, 2001.

18. **Khir AW, O'Brien A, Gibbs JS, and Parker KH.** Determination of wave speed and wave separation in the arteries. *J Biomech* 34: 1145–1155, 2001.
19. **Khir AW and Parker KH.** Measurements of wave speed and reflected waves in elastic tubes and bifurcations. *J Biomech* 35: 775–783, 2002.
20. **Koh TW, Pepper JR, DeSouza AC, and Parker KH.** Analysis of wave reflections in the arterial system using wave intensity: a novel method for predicting the timing and amplitude of reflected waves. *Heart Vessels* 13: 103–113, 1998.
21. **Liang YL, Teede H, Kotsopoulos D, Shiel L, Cameron JD, Dart AM, and McGrath BP.** Non-invasive measurements of arterial structure and function: repeatability, interrelationships and trial sample size. *Clin Sci (Colch)* 95: 669–679, 1998.
22. **MacRae JM, Sun YH, Isaac DL, Dobson GM, Cheng CP, Little WC, Parker KH, and Tyberg JV.** Wave-intensity analysis: a new approach to left ventricular filling dynamics. *Heart Vessels* 12: 53–59, 1997.
23. **Milnor WR.** *Hemodynamics*. Baltimore, MD: Williams & Wilkins, 1989.
24. **Nichols WW and O'Rourke MF.** Sphygmocardiography. In: *McDonald's Blood Flow in Arteries. Theoretical, Experimental and Clinical Principles.* London: Edward Arnold, 1998, p. 444–476.
25. **Nichols WW and O'Rourke MF.** *McDonald's Blood Flow in Arteries. Theoretical, Experimental and Clinical Principles.* London: Edward Arnold, 1998.
26. **Nichols WW and O'Rourke MF.** Principles of recording and analysis of arterial waveforms. In: *McDonald's Blood Flow in Arteries. Theoretical, Experimental and Clinical Principles*. London: Edward Arnold, 1998, p. 223–242.
27. **Nichols WW and O'Rourke MF.** Wave reflections. In: *McDonald's Blood Flow in Arteries. Theoretical, Experimental and Clinical Principles*. London: Edward Arnold, 1998, p. 201–222.
28. **Niki K, Sugawara M, Chang D, Harada A, Okada T, Sakai R, Uchida K, Tanaka R, and Mumford CE.** A new noninvasive measurement system for wave intensity: evaluation of carotid arterial wave intensity and reproducibility. *Heart Vessels* 17: 12–21, 2002.
29. **Niki K, Sugawara M, Uchida K, Tanaka R, Tanimoto K, Imamura H, Sakomura Y, Ishizuka N, Koyanagi H, and Kasanuki H.** A noninvasive method of measuring wave intensity, a new hemodynamic index: application to the carotid artery in patients with mitral regurgitation before and after surgery. *Heart Vessels* 14: 263–271, 1999.
30. **Nobuoka S, Aono J, Nagashima J, Ando H, Adachi H, Imai Y, Shibamoto M, Tanaka H, Miyake F, and Murayama M.** Assessment of reflection pulse wave in patients with cardiomyopathy: evaluation of noninvasive measurement of wave intensity. *Acta Cardiol* 56: 283–287, 2001.
31. **O'Brien E, Mee F, Atkins N, and Thomas M.** Evaluation of three devices according to the revised British Hypertension Society Protocol: the Omron HEM-705CP, Phillips HP5332, and Nissei DS-175. *Blood Pressure Monitoring* 1: 55–61, 1996.
32. **O'Rourke MF.** Vascular impedance in studies of arterial and cardiac function. *Physiol Rev* 62: 570–623, 1982.
33. **Parker KH and Jones CJ.** Forward and backward running waves in the arteries: analysis using the method of characteristics. *J Biomech Eng* 112: 322–326, 1990.
34. **Parker KH, Jones CJ, Dawson JR, and Gibson DG.** What stops the flow of blood from the heart? *Heart Vessels* 4: 241–245, 1988.
35. **Ramsey MW and Sugawara M.** Arterial wave intensity and ventriculo-arterial interaction. *Heart Vessels Suppl* 12: 128–134, 1997.
36. **Rickey DW and Fenster A.** Evaluation of an automated real-time spectral analysis technique. *Ultrasound Med Biol* 22: 61–73, 1996.
37. **Rimoy GH, Bhaskar NK, and Rubin PC.** Reproducibility of Doppler blood flow velocity waveform measurements: study on variability within and between day and during hemodynamic intervention in normal subjects. *Eur J Clin Pharmacol* 41: 125–129, 1991.
38. **Routh HF, Powrie CW, and Peterson RB (Inventors); Advanced Technology Laboratories (Assignee).** *Continuous Display of Peak and Mean Blood Flow Velocities.* US Patent 5,287,753. 22 Feb. 1994. Int. cl. G01F 001/00.
39. **Segers P and Verdonck P.** Role of tapering in aortic wave reflection: hydraulic and mathematical model study. *J Biomech* 33: 299–306, 2000.
40. **Shau YW, Wang CL, Shieh JY, and Hsu TC.** Noninvasive assessment of the viscoelasticity of peripheral arteries. *Ultrasound Med Biol* 25: 1377–1388, 1999.
41. **Sokolow M, McIlroy MB, and Cheitlin MD.** Clinical physiology. In: *Clinical Cardiology*. East Norwalk, CT: Appleton & Lange, 1990, p. 69–86.
42. **Sun YH, Anderson TJ, Parker KH, and Tyberg JV.** Wave-intensity analysis: a new approach to coronary hemodynamics. *J Appl Physiol* 89: 1636–1644, 2000.
43. **Zambanini A, Khir AW, Byrd SM, Parker KH, Thom SA, and Hughes AD.** Wave intensity analysis: a novel non-invasive method for determining arterial wave transmission. *Computers in Cardiology* 29: 717–720, 2002.
44. **Zambanini A, Khir AW, Parker KH, Thom SA, and Hughes AD.** Calibration of an arterial applanation tonometer for in-vivo pressure transduction. *Proc IV World Congr Biomechan,* 2002.
45. **Zwiebel WJ.** Doppler frequency spectrum analysis. In: *Introduction to Vascular Ultrasonography*, edited by Zwiebel WJ. Philadelphia, PA: Saunders, 2000, p. 45–66.